Proper Motions of the HH 47 Jet Observed with the Hubble Space Telescope [1]

Patrick Hartigan [2], Steve Heathcote [3], Jon A. Morse [4], Bo Reipurth [5],

and John Bally [6]

arXiv:astro-ph/0507526v1 22 Jul 2005

[1]Based on observations made with the NASA/ESA *Hubble Space Telescope*, obtained at the Space Telescope Science Institute, which is operated by the Association of Universities for Research in Astronomy, Inc., under NASA contract NAS5-26555.

[2]Dept. of Physics and Astronomy, Rice University, 6100 S. Main, Houston, TX 77251-1892

[3]Cerro Tololo Interamerican Observatory, NOAO, Casilla 603, La Serena, Chile

[4]Dept. of Physics and Astronomy, Arizona State University, Tempe AZ

[5]Institute for Astronomy, University of Hawaii, 640 N. Aohoku Place, Hilo HI 96720

[6]Center for Astrophysics and Space Astronomy, 389 UCB, University of Colorado, Boulder, CO 80309, USA

ABSTRACT

We present a proper motion study of the shock waves within the classic stellar jet HH 47 based on Hubble Space Telescope Hα and [S II] images of the region taken over two epochs. Individual knots within the jet and in the bow shock/Mach disk working surface of HH 47A move significantly in the five years that separate the images, and the excellent spatial resolution of HST makes it possible to measure the proper motions with enough precision to easily observe differential motions throughout the flow. The bright portion of the jet emerges at 37.5 $\pm$ 2.5 degrees from the plane of the sky with an average velocity of 300 km s^{-1}. Dynamical ages of the shock waves in the jet range from a few decades for knots recently ejected by the source to $\sim$ 1300 years for the faint extended bow shock HH 47D. The jet curves, but motions of knots in the jet are directed radially away from the exciting source, and velocity variability in the flow drives the shock waves that heat the jet internally. The jet orientation angle varies with time by about 15 degrees, and currently points to the northwestern portion of a cavity outlined by a reflection nebula, where a quasi-stationary shock deflects the jet. The major working surface HH 47A is more complex than a simple bow shock/Mach disk, and contains numerous clumps that move relative to one another with velocities of $\sim$ $\pm$ 40 km s^{-1}. Small clumps or instabilities affect the Mach disk, and dense clumps may move all the way through the working surface to cause the bumpy morphology seen at the bow shock. A localized area between the bow shock and Mach disk varies significantly between the two sets of images.

1.   INTRODUCTION

Since their discovery in the mid-1980's, collimated jets from young stars have played an increasingly important role in clarifying how stars form. Jets provide a means for protoplanetary disks to shed angular momentum as disk material accretes onto the star, and recent observations of rotation in jets provide a direct observational link to the accretion disk that ultimately powers these flows (Coffey et al. 2004). Most stars are members of binaries, and jets provide crucial information about disks in such systems through measurements of precession (Gómez et al. 1997), and by tracing separate flows from both components of close binaries (Reipurth et al. 1999; Hartigan & Kenyon 2003). Jets evacuate large cavities that pierce the surrounding molecular cloud and power large-scale bipolar molecular outflows which help to support molecular clouds against gravitational collapse (Reipurth & Bally 2001). Because outflows are driven by accretion, knots in jets give a fossil record of the accretion history of young stars. Collimated outflows also accompany accretion disks in compact galactic sources (Mirabel & Rodriguez 1999), and in extragalactic nuclei (Zensus 1997); jets from young stars are a particularly good place to study the connection between accretion and outflow because shock waves in the flow cool radiatively, so images and spectra reveal where the flows are heated and trace how they propagate.

The excellent spatial resolution provided by the Hubble Space Telescope has greatly advanced our understanding of jet dynamics. Cooling zones behind shock waves in stellar jets are typically near the limit of what can be resolved from the ground, but these zones are clearly resolvable with *HST*. Shock waves in nearby jets move ~ 1 arcsecond per decade, but also change their spatial structure on that timescale. Hence, the subarcsecond spatial resolution provided by *HST* makes it possible to detect real differential motions between jet knots, and thereby observe the complex dynamics of working surfaces, merging bow shocks, and fluid instabilities in real time. It is possible to observe the true density structure and

calculate mass loss rates directly when jets are irradiated by ultraviolet light (Yusef-Zadeh et al. 2005).

The three bright stellar jets (HH 1, HH 34, and HH 111) we have observed to date in this manner each reveal something new and unexpected about the dynamics of jets from young stars. A portion of the large bow shock HH 34 (Reipurth et al. 2002) appears to be in the process of forming a Rayleigh-Taylor instability, and we observed new shock waves form as dense knots emerged from the source. The proper motions in HH 111 (Hartigan et al. 2001) clearly show the aftermath of merging bow shocks, and faint emission wings along the shocks in the flow demonstrate that the surrounding material plays no role in collimating the jet once the jet emerges from the source. Because HH 111 is in the plane of the sky, the proper motions are the true space velocities, so here we can observe the actual velocity variations in the flow and thereby test models of radiative shocks in jets. A remarkable area of strong shear exists along the edges of the bow shock HH 1, while the flow is much more complex and less ordered on the opposite side of the flow in HH 2 (Bally et al. 2002).

Discovered by Schwartz (1977), the famous HH 46/47 bipolar outflow is in many ways an ideal object to study jet dynamics. The jet is bright, and shows a classic structure of a collimated flow with several large bow shocks. The brightest bow shock, HH 47A, is one of the best examples of a working surface, and Hα images of the system taken with *HST* (Heathcote et al. 1996, hereafter H96) reveal a distinct bow shock that accelerates downstream material and a Mach disk that decelerates incident jet gas. The star formation in the region is relatively simple – the jet emanates from a resolved ($\sim 0\rlap{.}''26$) low mass binary system surrounded by a circumstellar disk (Reipurth et al. 2000) that has formed in the isolated Bok globule ESO 210-6A at the edge of the Gum Nebula. This binary is the only known young stellar system in the globule. The globule is clearly compressed to the north and west toward the source of ionizing radiation (Figure 1 of H96). The nascent

stellar system and circumstellar disk are thus transitioning from being embedded in the dense globule to being exposed to the UV radiation from the nearby massive stars ζ Pup and γ^2 Vel through photoevaporation of the surrounding envelope (Reipurth 1983).

The HH 46/47 outflow has been studied extensively across the electromagnetic spectrum at UV, optical, and infrared wavelengths (H96; Hartigan et al. 1999; Reipurth & Heathcote 1991; Chernin & Masson 1991; Eislöffel et al 1994; Noriega-Crespo et al. 2004). The optically bright HH 46/47 jet is part of the northeast flow, and terminates in the HH 47A bow shock $\sim 1.3'$ from the IR driving source. HH 47A moves outward in the wake of the larger, fainter bow shock HH 47D. A faint counterjet in the redshifted southwest lobe (Eislöffel & Mundt 1994) extends toward the bow shock HH 47C (Dopita et al. 1982). Assuming a distance of 450 pc (Eggen 1980; Claria 1982), the visible outflow from HH 47D to HH 47C extends $\sim$0.57 pc. The outflow velocities of $\sim$300 km s^{-1} derived from proper-motion and radial-velocity studies (Hartigan et al. 1990; Reipurth & Heathcote 1991; Eislöffel & Mundt 1994; Micono et al. 1998; Schwartz & Greene 2003) imply a kinematical age for the main optical/near-IR outflow of $\sim 10^3$ years, with large mass ejections occuring every 400 years or so (Morse et al. 1994), perhaps driven by FU Orionis-type eruptions (Dopita 1978). However, as occurs with other HH flows (e.g. HH 34 Bally & Devine 1994), deep wide field images reveal that HH 46/47 extends at least 2.6 pc from the IRS, and therefore must be $\gtrsim 10^4 - 10^5$ years old (Stanke et al. 1999).

In this paper we continue our investigation of stellar jet dynamics by presenting *HST* proper motions of the optically emitting shocks in the HH 46/47 jet. The new observations were taken about 5 years after those in H96, long enough for knots in the jet to move significantly, but short enough that morphological changes remain small for most of the knots. In addition to being able to quantify precession and differential motions in the jet with high precision, the new images make it possible to study the dynamics of a working

surface in exquisite detail for the first time.

2. OBSERVATIONS AND DATA REDUCTION

We imaged the HH 47 jet through the F656N and the F673N filters with the WFPC-2 camera on *HST* on 26 February 1999, a time interval of 4.9 years after the first epoch of images described by H96. The images include the entire bright jet on one WF chip, with the extended bow shock HH 47D spread across the PC (Fig. 1). Three exposures each for Hα and [S II] facilitated cosmic-ray removal. Total exposure times for the Hα and [S II] images in the 1999 epoch were 4100 seconds and 4000 seconds, respectively. We reduced the new images and aligned them with the previous epoch using the same procedures described in H96.

A difference image between the two epochs (Fig. 2) shows clearly that the jet and bow shocks move away from HH 47-IRS. To measure proper motions we used a method described by Currie et al. (1996), explained in more detail in Hartigan et al. (2001). The algorithm shifts two images to minimize the square of the difference of the counts over a region that defines the object. We examined each image for features that retained their overall shape between the two epochs and applied the procedure separately for Hα and for [S II], because HH objects often have different morphologies when imaged in these two filters. Figs. 3 and 4 show objects in the jet, while Figs. 5 and 6 cover the HH 47A bow shock. Variable features within HH 47A are emphasized in Fig. 7. Table 1 compiles proper motions of all the objects identified in the figures. Coordinates in the table were obtained using the stsdas task xy2rd.

Errors in the proper motions come from imperfect alignment of the images between epochs, uncertainties in the centroiding routine that determines the spatial shifts, and errors

in the distance to HH 47. In the HH 47 images there are many field stars available to align the epochs, so uncertainties in the registration are small. Using the proper motion code on stars after the images were aligned shows the rms error in the image registration is about 0.1 pixel. Formal statistical errors in centroiding features are typically 0.05 pixel. However, an additional systematic error of ~ 0.1 pixel arises from using different buffer sizes to search for the centroid (e.g. H96). The distance to HH 47 derives from estimates of the distance to NGC 2547 (450 pc Claria 1982) and to a group of coeval stars within about 5 degrees of the Vela pulsar (425 pc Eggen 1980). The projected distance of HH 47 from NGC 2547 is about 3 degrees, or 25 pc at a distance of 450 pc. We adopt 25 pc as the uncertainty in the distance, which introduces a 6% error in the observed tangential velocities.

Altogether, internal errors in the proper motions over the 4.9 year interval between epochs are $\sim 5 \ \mathrm{km\,s^{-1}}$, for all objects except the large, diffuse bow shock HH 47D, where the uncertainty is 40 $\mathrm{km\,s^{-1}}$. The 6% uncertainty in the distance is a multiplicative constant that affects all the measurements in the same way. Proper motions in HH 47D derive from the sum of the Hα and [S II] images to improve the signal-to-noise.

3. PROPER MOTIONS, VARIABILITY, CLUMPY FLOW, AND THE CAVITY OF THE HH 47 JET

When combined with existing radial velocity information, our new proper motion measurements make it possible to calculate the orientation of the flow, its true space velocity, and to assess the degree to which clumpy flows and variations in the intrinsic velocity and in the ejection angles affect the jet dynamics. Initial results from the analysis of these data were reported by Hartigan (2003). Radial velocities along the jet observed by Meaburn & Dyson (1987, their Fig. 2) increase from HH46 IRS out to the HH 47A bow shock, and we observe the same behavior in the proper motions shown in Fig. 8.

This correlation between radial velocities and proper motions implies that the jet varies intrinsically in velocity. The alternative explanation, that changes in the ejection angles cause the radial velocities and proper motions to change, is ruled out because in this model proper motions increase as radial velocities decrease and vice-versa for a constant velocity flow.

The relatively poor spatial resolution of the ground-based radial velocity measurements makes it difficult to compare these directly with proper motions of specific emission features observed by *HST*. However, it is easy to identify the maximum radial velocity of the jet with respect to the cloud as being 200 ± 10 km s^{-1} before the jet encounters HH 47A (Meaburn & Dyson 1987; Hartigan et al. 1990). We measure the proper motion of knot Ah1 to be 300 $\pm$ 18 km s^{-1} (where the error is dominated by uncertainties in the distance), so this feature moves at an angle of 34 ± 2 degrees from the plane of the sky, with a velocity of 360 ± 28 km s^{-1}.

Because the jet is not straight, a long slit may miss some of the line emission in specific features and thereby give misleading estimates for the orientation angles. To obtain radial velocities for the entire emitting region one can use a slit map or observe with a Fabry-Perot, as was done by Morse et al. (1994). Using the datacube from that paper, the average radial velocity of the jet with respect to the cloud is 180 ± 10 km s^{-1}. The average proper motion of the jet in Fig. 8 is 235 km s^{-1}, with an intrinsic scatter of 10 km s^{-1} and a systematic error of 14 km s^{-1} from the distance. Hence, the average orientation angle of the jet with respect to the plane of the sky is 37.5 ± 2.5 degrees, in good agreement with the above measurement of Ah1 and with previous estimates from ground-based proper motions (Eislöffel & Mundt 1994).

As the last column of Table 1 shows, the outer bow shock HH 47D is about 1300 years old, and HH 47A was ejected a little less than 800 years ago, assuming no significant

deceleration of these objects has occurred. The average proper motion is ~ 235 km s^{-1} in the jet, ~ 200 km s^{-1} in HH 47A and ~ 180 km s^{-1} in HH 47D, so if this decline is caused by deceleration rather than source variability, then the amount of deceleration over the length of the jet is rather small compared with the velocity of the flow. The youngest knots in the jet are only a few decades old, and these knots have significantly higher proper motions than those ejected $150 - 200$ years ago.

The HH 47 flow is an excellent place to observe how a jet with a variable ejection angle clears out a larger cavity. The inner 20 arcseconds of the HH 47 jet curves to the left in Figs. 1 and 2, but the proper motions are not along the jet. Instead, the knots in the jet move away from the source radially, as expected for a jet with a variable ejection angle. The current direction of the jet, defined by the motion of knots Jh1, Jh2, and Js2, is more northerly than its average over the past millennium. The reflection nebula along the cavity is also brighter on the northern side, as if the space between the IRS and the northern cavity wall has been mostly cleared of dust, and Fig. 2 shows that this wall brightened between 1994 and 1999. There is direct evidence that the jet currently collides with stationary material on this side of the cavity. A morphologically variable, but stationary, linear Hα feature noted by H96 has the spatial position and orientation expected if the jet were impacting the northern edges of the cavity obliquely. It is now possible to study deflection shocks in laboratory experiments that propagate jets into crosswinds (Lebedev et al. 2004). The HH 46/47 deflection shock is present only in Hα, and is marked in Fig. 3.

Shocks in stellar jets are caused by faster material overtaking slower material (e.g. Hartigan et al. 2001). Typical velocity variations along the HH 47 jet between adjacent knots are ~ 20 km s^{-1}, with a few cases up to 40 km s^{-1}, in agreement with shock models of the emission line ratios (Hartigan et al. 1994). Two places in the flow will experience higher shock velocities in the future – proper motions in knot Ah1 exceed those of HH 47A by

about 100 $\mathrm{km\,s^{-1}}$, so the true impact velocity should be ~ 125 $\mathrm{km\,s^{-1}}$ when this knot enters the working surface in about the year 2040. This impact velocity should be large enough to generate [O III] line emission. The other area where proper motions change markedly is close to the source, where knots Jh1 and Jh2 have proper motions ~ 100 $\mathrm{km\,s^{-1}}$ higher than Jh3 and other knots ahead in the flow. The first dynamical consequence of these large proper motions should be in about 30 years, when these knots encounter the current position of the deflection shock (Fig. 3).

HH 47A appears as a bow shock with a well-defined Mach disk (Ah4 in Fig. 5), and models of HH 47A have attempted to predict the emission line ratios and line widths using this scenario. Based on the lack of [O III] $\lambda5007$, the shock velocities in HH 47A are $\lesssim 90$ $\mathrm{km\,s^{-1}}$ (Morse et al. 1994), and the bow shock model that fits the line widths and the entire optical/UV spectrum the best is one where the bow shock has a velocity of 60 $\mathrm{km\,s^{-1}}$ and the Mach disk 40 $\mathrm{km\,s^{-1}}$ (Hartigan et al. 1999). While these shock velocities are generally consistent with the new proper motion data, it is clear that the dynamics within HH 47A is more complex than a simple bow shock/Mach disk structure. Figs. 5, 6, and 8 show that individual clumps within HH 47A have different proper motions, and spread ± 40 $\mathrm{km\,s^{-1}}$ or so relative to the mean motion of HH 47A. For example, knot Ah8 clearly moves faster than the adjacent knot Ah10 (Fig. 7), and Table 1 confirms a relative velocity of ~ 40 $\mathrm{km\,s^{-1}}$ for these two knots.

Arrows in Fig. 7 mark two areas on the Mach disk that have changed over the five years between the epochs. The changes could result from some sort of fluid instability, or could simply arise when a small dense blob like Ah8 plunges through the Mach disk. The area between the bow shock and the Mach disk is particularly variable in Fig. 7. In general, Hα, where the flux is determined largely by collisional excitation at the shock and so is proportional to the mass flux across the shock at any given moment, traces morphological

changes more quickly than does [S II], which radiates in a spatially extended zone that averages changes out over a cooling time of tens of years.

4. CONCLUSIONS

We have measured precise proper motions from two epochs of *HST* images of the prototypical stellar jet HH 47. Uncertainties of the relative proper motions between knots are typically $\pm$ 5 km s^{-1}, considerably lower than variations of the internal motions of the knots in the jet, so we can assess how the fluid dynamics operates in this system accurately for the first time.

Taking the source to be at a distance of 450 pc, the orientation angle of the flow is 37.5 $\pm$ 2.5 degrees with respect to the plane of the sky. The bright portion of the jet is about 800 years old, and has an average space velocity of 300 km s^{-1}. Although the jet curves, the motion is primarily directed radially away from the source. The ejection angle of the jet varies with time by $\pm$ 15 degrees or so, and currently impacts the northern side of the reflection nebula, where an oblique shock redirects the supersonic flow.

Proper motions in the jet increase with distance along the bright section of the jet in front of the bow shock HH 47A, similar to the behavior of radial velocities. This correlation implies that the source varies intrinsically in velocity, and it is these velocity variations that produce shocks that heat the jet internally. The observed variations in proper motion along the jet are consistent with shock models that were designed to explain the observed emission line ratios in the jet.

The bright bow shock HH 47A has a clear Mach disk and bow shock, but the object is more complex than a dual shock structure, and has many clumps whose differential motions dominate much of the dynamics in this object. The region between the bow

shock and Mach disk has a highly variable morphology, and the Mach disk also changed structure significantly over the five year interval between images. The individual knots within HH 47A are easiest to explain as small bullets that pass from the jet through the Mach disk and working surface to emerge as bumps in the bow shock.

Understanding HH flow dynamics will require systematic work that spans decades, but the rewards are great because these objects make it possible to test our basic understanding of the time dependences of shocked supersonic flows, a ubiquitous phenomenon in astrophysics. Additional epochs of high spatial resolution imaging of HH 47 will be able to follow the dynamics of this fascinating object in real time, and thereby provide ideal constraints for numerical models of working surfaces within collimated supersonic flows.

REFERENCES

Bally, J., & Devine, D. 1994, ApJ 428, L65

Bally, J., Heathcote, S., Reipurth, B., Morse, J., Hartigan, P., & Schwartz, R. D. 2002, AJ 123, 2627

Chernin, L., & Masson, C. R. 1991, ApJ 372, 646

Clariá, J. 1982, A&AS 47, 323

Coffey, D., Bacciotti, F., Woitas, J., Ray, T. P., & Eislöffel, J. 2004, ApJ 604, 758

Currie, D. G., et al. 1996, AJ 112, 1115

Dopita, M. A. 1978, ApJS 37, 117

Dopita, M. A., Schwartz, R. D., & Evans, I. 1982, ApJ 263, L73

Eislöffel, J., Davis, C. J., Ray, T. P., & Mundt, R. 1994, ApJ 422, L91

Eislöffel, J., & Mundt, R. 1994, A&A 284, 530

Eggen, O. 1980, ApJ 238, 627

Gómez, M., Kenyon, S., & Whitney, B. 1997, AJ 114, 265

Graham, J. A., & Heyer, M. H. 1989, PASP 101, 573

Hartigan, P., Raymond, J., & Meaburn, J. 1990, ApJ 362, 624

Hartigan, P., Morse, J., & Raymond, J. 1994, ApJ 436, 125

Hartigan, P., Morse, J., Tumlinson, J., Raymond, J., & Heathcote, S. 1999, ApJ 512, 901

Hartigan, P., Morse, J., Heathcote, S., Reipurth, B., & Bally, J. 2001, ApJ 559, L157

Hartigan, P. & Kenyon, S. 2003, ApJ 583, 334

Hartigan, P. 2003, Ap&SS 287, 111

Heathcote, S. Morse, J., Hartigan, P., Reipurth, B., Schwartz, R., Bally, J., & Stone, J. 1996, AJ 112, 1141 [H96]

Lebedev, S. et al. 2004, ApJ 616, 988

Meaburn, J., & Dyson, J. 1987, MNRAS 225, 863

Mirabel, I., & Rodriguez, L. 1999, ARA&A 37, 409

Micono, M., Davis, C. J., Ray, T. P., Eislöffel, J., & Shetrone, M. D. 1998, ApJ 494, L227

Morse, J. A., Hartigan, P., Heathcote, S., Raymond, J., & Cecil, G. 1994, ApJ 425, 738

Noriega-Crespo, A., et al. 2004, ApJS 154, 352

Reipurth, B. 1983, A&A 117, 183

Reipurth, B., & Bally, J. 2001, ARA&A 39, 403

Reipurth, B., & Heathcote, S. 1991, A&A 246, 511

Reipurth, B., Heathcote, S., Morse, J., Hartigan, P., & Bally, J. 2002, AJ 122, 3419

Reipurth, B., Yu, K., Heathcote, S., Bally, J., & Rodriguez, L. 2000, AJ 120, 1449

Reipurth, B., Yu, K., Rodriguez, L., Heathcote, S., & Bally, J. 1999, A&A 352, L83

Schwartz, R. D. 1977, ApJ 212, L25

Schwartz, R. D., & Greene, T. P. 2003, AJ 126, 339

Stanke, T., McCaughrean, M. J., & Zinnecker, H. 1999, A&A 350, L43

Yusef-Zadeh, F., Biretta, J., & Wardle, M. 2005, ApJ 624, 246

Zensus, J. 1997, ARA&A 35, 607

Table 1.   Proper Motions in HH 47

Object[a]	α (2000)[b]	δ (2000)[b]	ΔX[c]	ΔY[c]	$V_{X\perp}$[d]	$V_{Y\perp}$[d]	$V_{\perp}$[d]	Age[e]
Jh1	8:25:44.009	−51:00:33.49	117	36	249	76	261	19
Jh2	8:25:44.154	−51:00:32.27	124	32	264	68	273	32
Jh3	8:25:44.826	−51:00:25.10	80	22	170	46	176	166
Jh4	8:25:45.556	−51:00:22.40	89	−1	191	−3	191	229
Jh5	8:25:45.816	−51:00:23.60	95	6	203	13	204	228
Jh6	8:25:45.863	−51:00:21.42	100	14	214	30	217	231
Jh7	8:25:46.005	−51:00:19.93	102	8	219	17	219	247
Jh8	8:25:46.224	−51:00:17.81	103	1	220	2	220	275
Jh9	8:25:46.629	−51:00:14.06	96	6	205	12	205	350
Jh10	8:25:47.415	−51:00:13.17	111	15	237	31	239	359
Jh11	8:25:47.215	−51:00:08.11	85	35	181	75	196	456
Jh12	8:25:48.423	−50:59:59.35	129	10	275	20	276	436
Ah1	8:25:49.783	−50:59:52.42	139	16	297	34	299	505
<Ah>	8:25:50.262	−50:59:52.51	93	−2	199	−4	199	797
Ah2	8:25:50.146	−50:59:53.65	90	−12	192	−26	194	
Ah3	8:25:49.978	−50:59:50.69	103	10	221	22	222	
Ah4	8:25:50.156	−50:59:52.45	96	−7	206	−16	206	
Ah5	8:25:50.260	−50:59:52.87	79	6	169	12	169	
Ah6	8:25:50.466	−50:59:53.37	94	−14	201	−31	203	
Ah7	8:25:50.208	−50:59:50.34	89	−8	189	−16	190	
Ah8	8:25:50.307	−50:59:51.08	115	−4	244	−8	245	

Table 1—Continued

Object[a]	α (2000)[b]	δ (2000)[b]	Δ X[c]	Δ Y[c]	$V_{X\perp}$[d]	$V_{Y\perp}$[d]	$V_\perp$[d]	Age[e]
Ah9	8:25:50.360	−50:59:51.84	85	−5	182	−11	183	
Ah10	8:25:50.304	−50:59:50.42	96	−10	204	−21	205	
Ah11	8:25:50.424	−50:59:51.51	91	−8	195	−17	195	
Ah12	8:25:50.409	−50:59:50.77	98	−9	210	−18	211	
Js1	8:25:44.017	−51:00:33.83	125	32	267	68	276	16
Js2	8:25:44.816	−51:00:25.12	88	20	187	43	192	151
Js3	8:25:45.011	−51:00:24.17	114	18	243	38	246	135
Js4	8:25:45.312	−51:00:23.18	115	6	245	13	245	159
Js5	8:25:45.445	−51:00:21.19	96	3	204	7	204	215
Js6	8:25:45.532	−51:00:22.39	97	−2	207	−3	207	210
Js7	8:25:45.811	−51:00:23.53	94	5	200	10	200	232
Js8	8:25:45.688	−51:00:21.16	102	−7	219	−15	219	217
Js9	8:25:45.870	−51:00:21.43	102	15	218	32	220	227
Js10	8:25:46.031	−51:00:19.25	108	8	231	17	231	240
Js11	8:25:46.319	−51:00:17.95	108	2	230	5	230	269
Js12	8:25:46.697	−51:00:15.18	111	−2	236	−5	236	303
Js13	8:25:46.951	−51:00:15.06	114	−2	244	−5	244	311
Js14	8:25:47.274	−51:00:11.89	107	10	229	21	230	370
Js15	8:25:47.284	−51:00:08.15	116	3	248	7	248	364
Js16	8:25:47.655	−51:00:08.53	122	15	260	32	262	365
Js17	8:25:47.544	−51:00:06.02	118	5	251	12	251	387

Table 1—Continued

Object[a]	α (2000)[b]	δ (2000)[b]	Δ X[c]	Δ Y[c]	$V_{X\perp}$[d]	$V_{Y\perp}$[d]	$V_\perp$[d]	Age[e]
Js18	8:25:48.048	−51:00:02.95	118	4	252	9	252	434
Js19	8:25:48.482	−51:00:00.36	118	8	251	16	252	476
Js20	8:25:49.335	−50:59:55.84	133	1	283	2	283	492
As1	8:25:49.783	−50:59:52.42	140	−1	299	−1	299	505
<As>	8:25:50.254	−50:59:52.57	95	−5	203	−12	203	779
As2	8:25:50.199	−50:59:56.11	76	−4	162	−8	162	
As3	8:25:50.316	−50:59:56.31	92	5	196	11	197	
As4	8:25:50.284	−50:59:54.73	83	3	176	6	176	
As5	8:25:50.390	−50:59:55.87	92	−1	197	−2	197	
As6	8:25:50.379	−50:59:54.87	90	−7	192	−15	193	
As7	8:25:50.550	−50:59:54.54	91	−1	195	−2	195	
As8	8:25:50.477	−50:59:56.62	83	−7	178	−15	179	
As9	8:25:50.448	−50:59:54.45	98	−6	210	−12	210	
As10	8:25:50.475	−50:59:53.65	93	−8	198	−18	199	
As11	8:25:50.064	−50:59:50.49	102	6	218	13	218	
As12	8:25:50.187	−50:59:49.76	86	3	184	6	184	
As13	8:25:50.165	−50:59:54.43	94	−4	201	−9	201	
As14	8:25:50.118	−50:59:53.67	108	6	230	13	230	
As15	8:25:50.269	−50:59:52.92	85	8	182	17	183	
As16	8:25:50.380	−50:59:51.87	86	−13	184	−28	187	
As17	8:25:50.417	−50:59:51.27	99	−4	211	−8	211	

Table 1—Continued

Object[a]	α (2000)[b]	δ (2000)[b]	Δ X[c]	Δ Y[c]	$V_{X\perp}$[d]	$V_{Y\perp}$[d]	$V_\perp$[d]	Age[e]
As18	8:25:50.328	−50:59:51.04	111	−6	236	−12	236	
As19	8:25:50.314	−50:59:50.40	101	−11	216	−24	217	
As20	8:25:50.215	−50:59:51.59	67	10	143	21	144	
D	8:25:53.64	−50:59:32	84	0	179	0	179	1333

[a]Objects are defined by the boxes drawn in the figures. The labels J and A mean the object is in the jet or in HH 47A, respectively, and the letters h and s indicate the Hα, and [S II] images, respectively. The objects <Ah> and <As> are defined by large boxes that include all the emission that comprises HH 47A in the Hα, and [S II] images, respectively.

[b]Coordinates are for epoch 1994.24, and equinox 2000.

[c]Δ X and Δ Y are the proper motions in milliarcseconds per year along, and perpendicular to the axis of the jet, respectively. Positive values of Δ Y indicate motions to the right (to the NW) in the figures. The position angle of the jet on the sky is 54.18 degrees.

[d]Tangential velocity $V_{X\perp}$ along the x−direction, $V_{Y\perp}$ along the y−direction, and the total proper motion $V_\perp$ are in $km\,s^{-1}$, assuming a distance of 450 pc. Uncertainties are ± 5 $km\,s^{-1}$ for all objects except D, where they are ± 40 $km\,s^{-1}$. An additional systematic uncertainty of $\lesssim 6\%$ may arise from errors in the distance.

[e]Time in years for the object to move from the source to its present location at its current

velocity. The source position, $\alpha(2000) = $ 08:25:43.91, $\delta(2000) = -51$:00:35.6, is from an IRAC 2 Spitzer image (Noriega-Crespo 2005, personal communication).
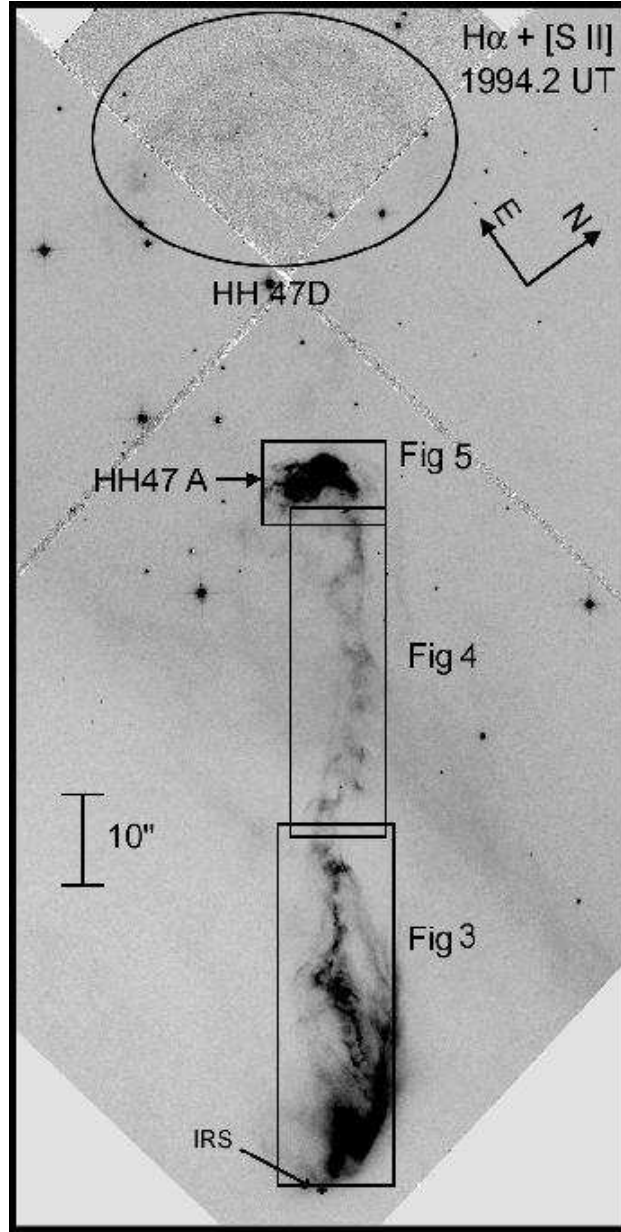
Fig. 1.— An image of the HH 47 jet created by adding together the [S II] and Hα WFPC2 images taken in 1994. The bow shocks HH 47D and HH 47A are indicated, and boxes show the areas covered by subsequent figures. A cross marks the position of the exciting source from the IRAC 2 Spitzer image (2005, Noriega-Crespo personal communication). The image is rotated to make the axis of the jet at PA = 54.18° vertical.
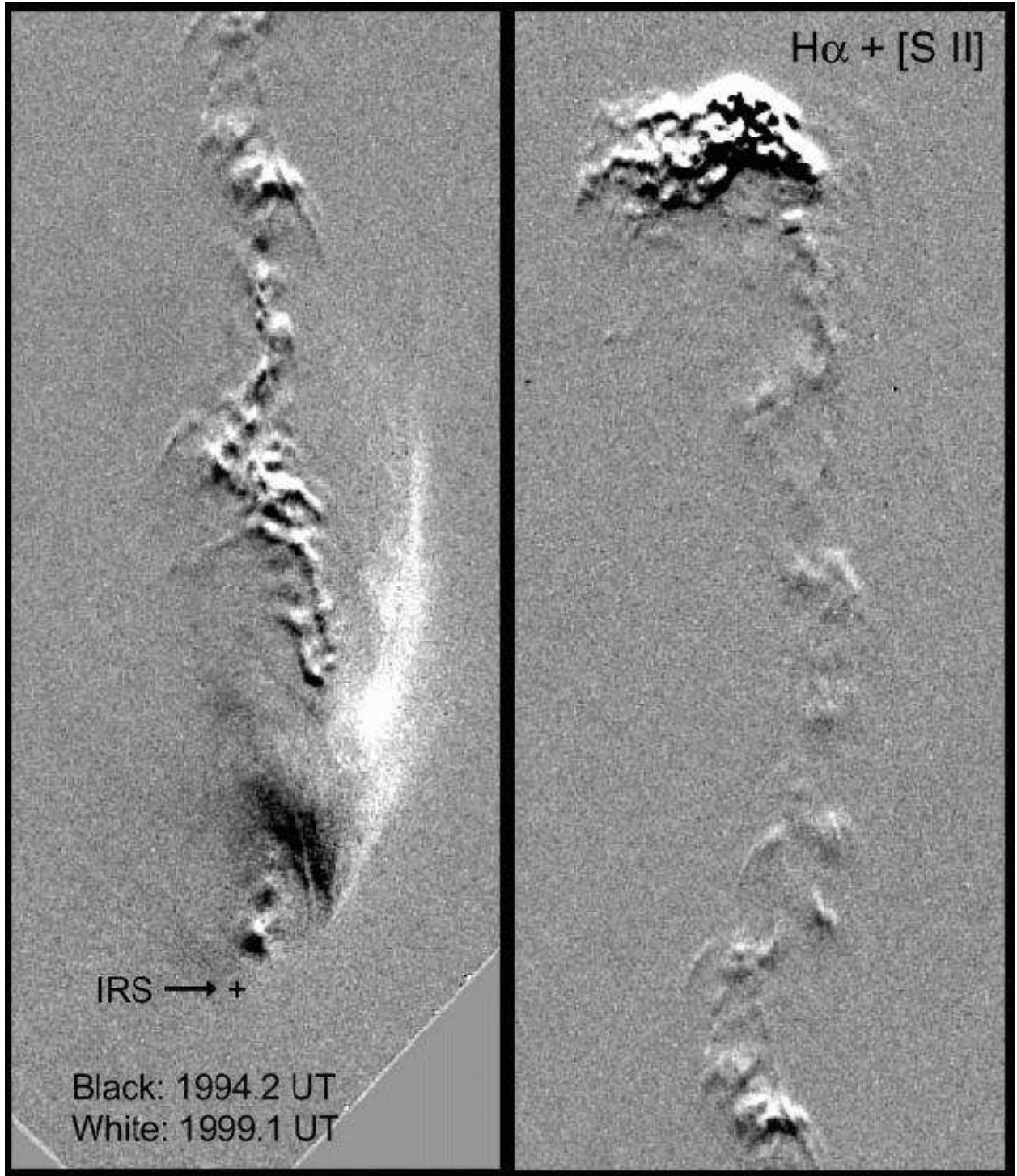
Fig. 2.— Difference between the 1994.2 UT (black) and the 1999.1 UT (white) epochs of the summed Hα + [S II] images of HH 47. Features in the jet move radially away from the infrared source (IRS), and so show a leading white edge and a trailing black edge. The reflection nebula near the base of the jet varied between the two epochs, becoming brighter on the northwest (right) side of the cavity in the second epoch.
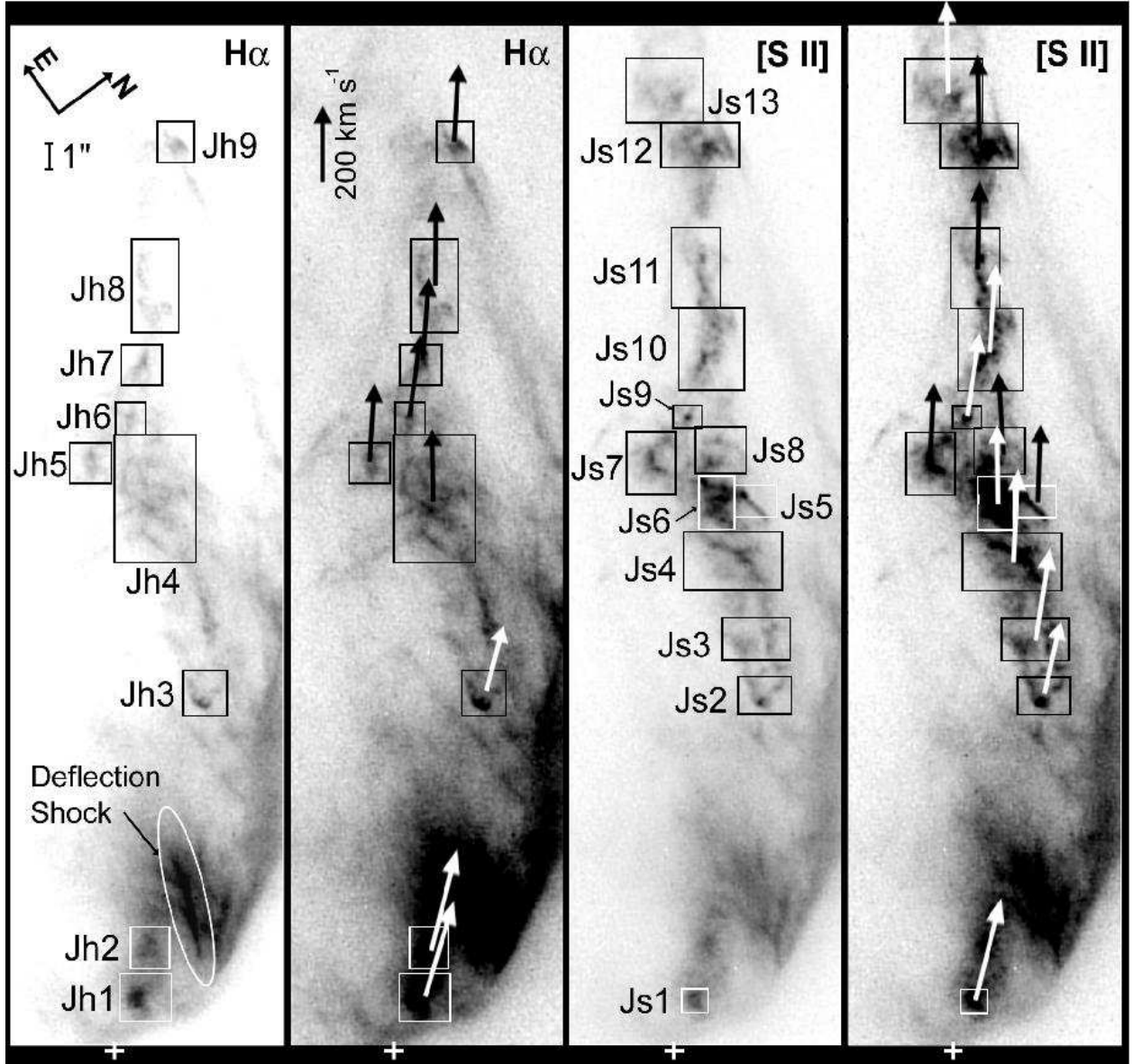
Fig. 3.— Proper motions in the lower section of the HH 47 jet. Boxes mark features used to measure proper motions in the Hα and [S II] images, each of which appears at two different greyscales for the 1994 epoch. Arrows denote the distance each feature would travel in 30 years. The curved structure on the right side of the image that extends from Jh1 to Jh9 is a reflection nebula. Crosses denote the IR source. The figure is oriented as in Fig. 1.
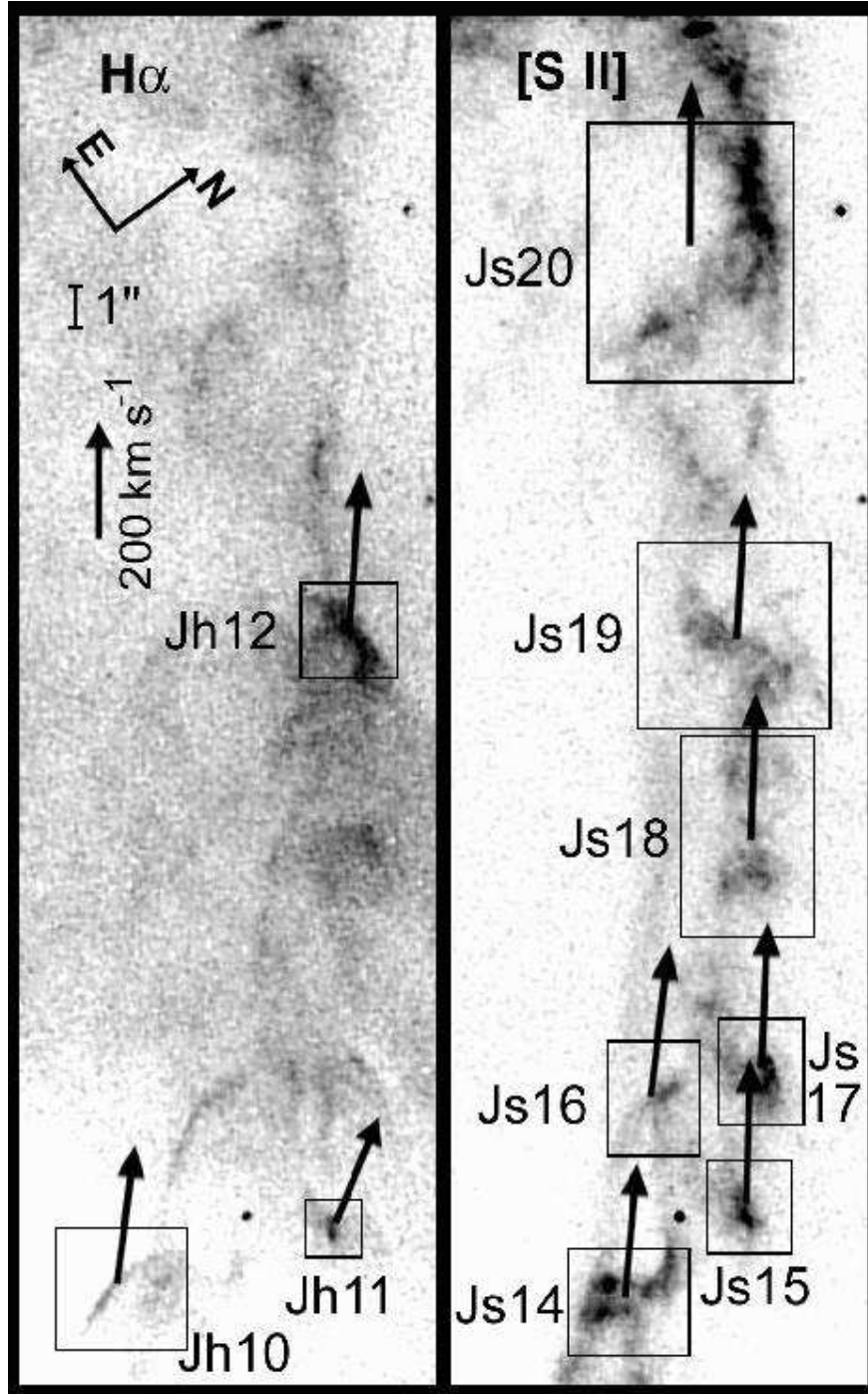
Fig. 4.— Same as Fig. 3 but for the middle portion of the jet.
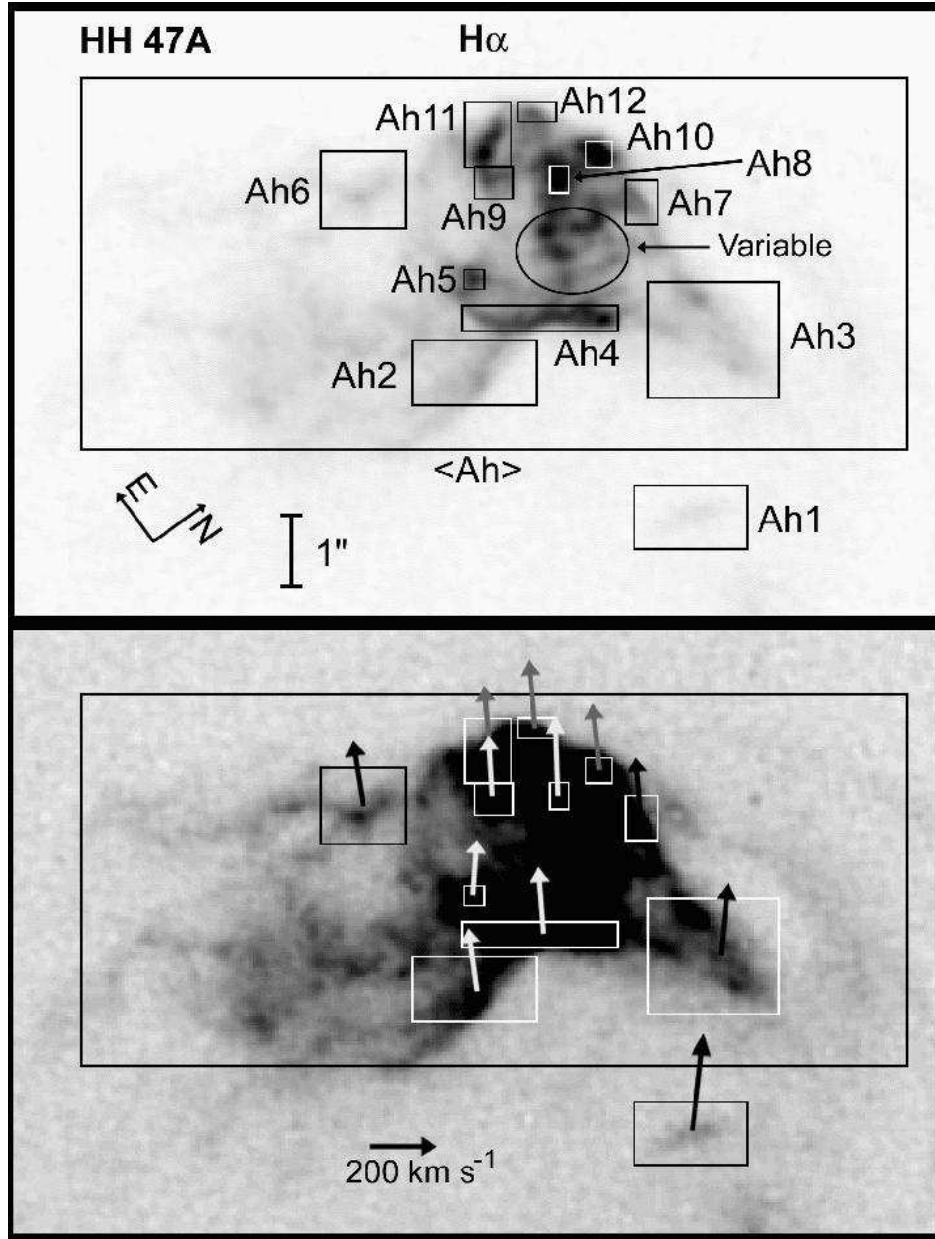
Fig. 5.— Same as Fig. 3 but for two greyscales of the 1994 Hα image of the HH 47A bow shock. In this case the arrows show the distance each feature would move in 10 years. The large box marked <Ah> includes emission from the entire structure. There are significant variations in the velocities between knots (see Table 1). Clumps within the region marked 'Variable' did not retain their shapes well enough to allow proper motion measurements between the two epochs.
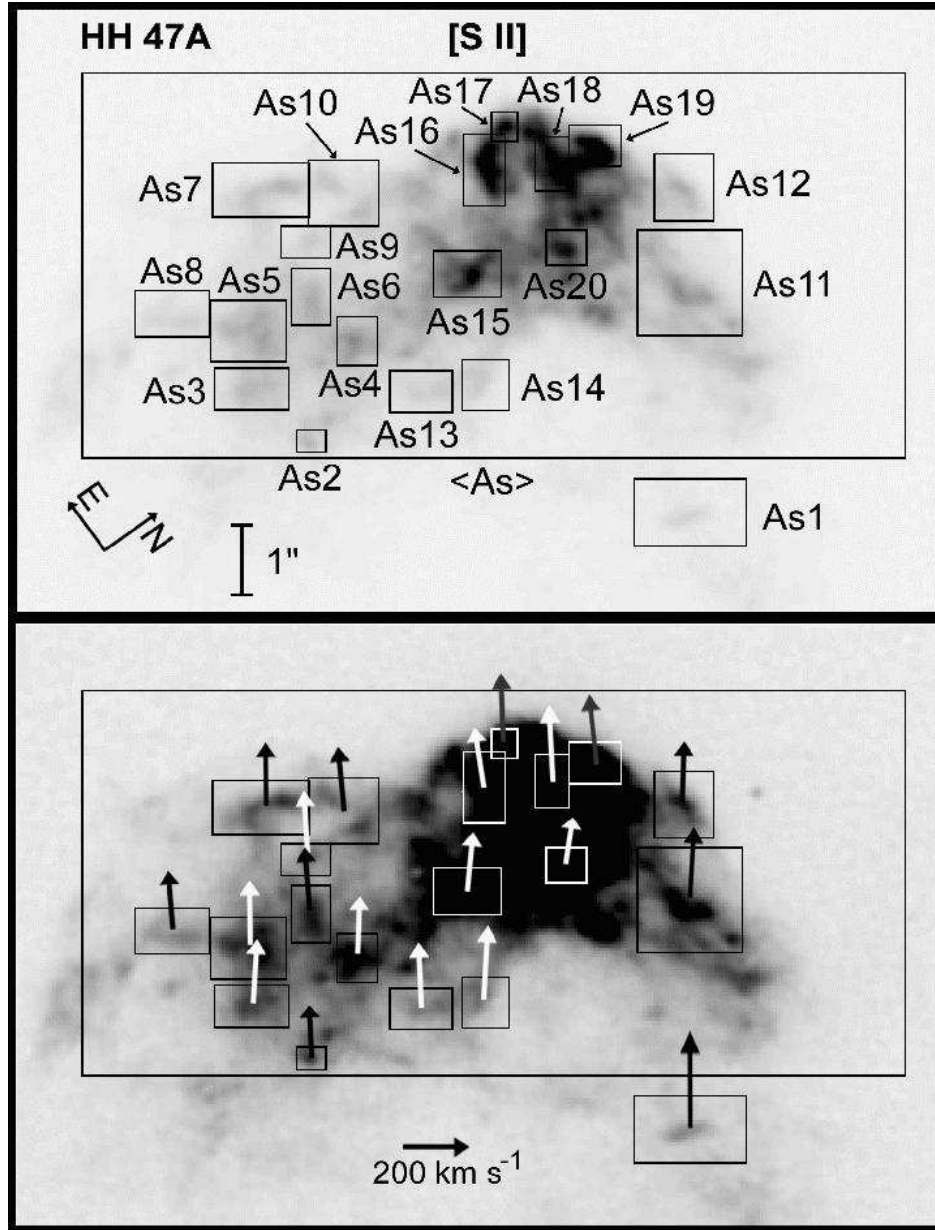
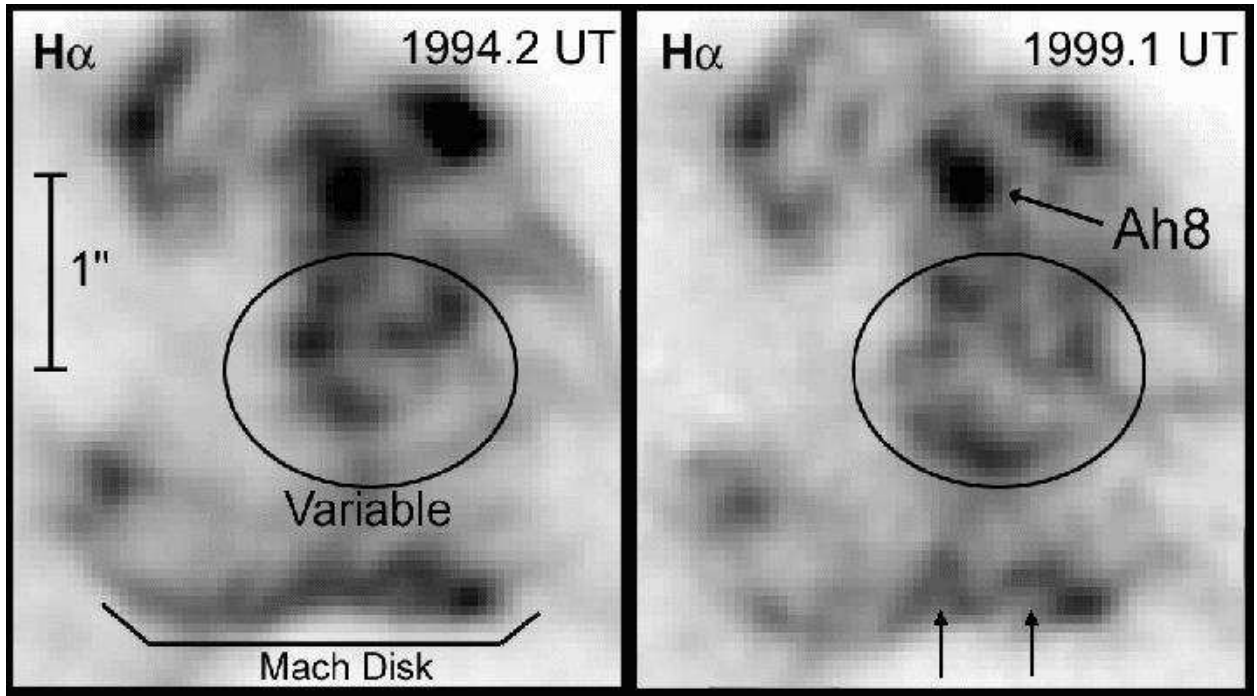Fig. 6.— Same as Fig. 5 for the HH 47A bow shock in [S II].

Fig. 7.— An expanded view of the variable region of HH 47A noted in Fig. 5. Two arrows at the bottom of the figure mark locations where the Mach disk changed its structure significantly. The 1999 epoch was shifted downward by an amount corresponding to a 200 $\mathrm{km\,s^{-1}}$ bulk motion over 4.9 years in order to align it with the 1994 epoch. The images clearly show the higher velocity of the bright knot Ah8 relative to the surrounding emission.
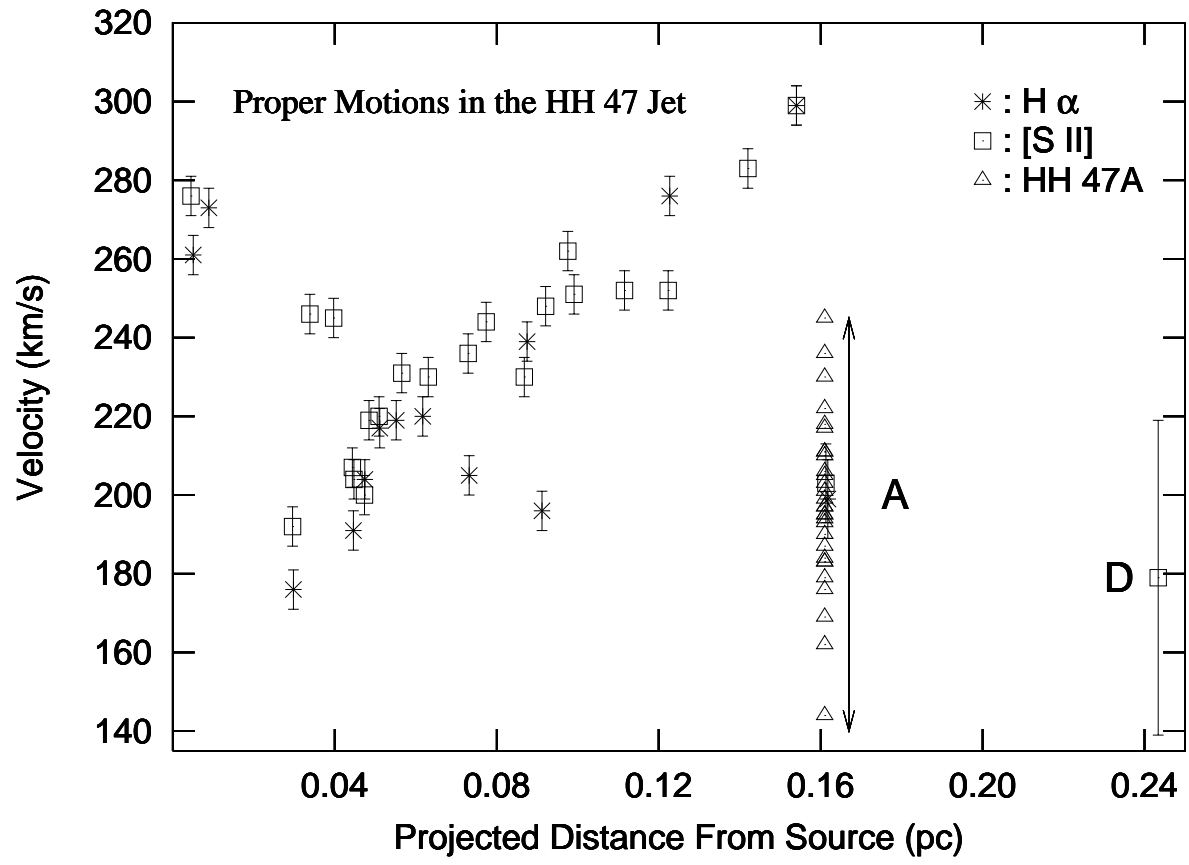
Fig. 8.—